
Stacked conductive metal–organic framework nanorods for high-performance vacuum electronic devices

Zhengxin Guan ^a, Jun Li ^{b,*}, Han Wu ^a, Xiaohong Chen ^a, Wei Ou-Yang ^{a,*}

^a Engineering Research Center for Nanophotonics & Advanced Instrument, Ministry of Education, School of Physics and Electronic Science, East China Normal University, 500 Dongchuan Road, Shanghai 200241, China.

^b Department of Electronic Science and Technology, Tongji University, 4800 Caoan Road, Shanghai 201804, China.

* Corresponding authors: jun_li@tongji.edu.cn, ouyangwei@phy.ecnu.edu.cn

Abstract

Metal-organic frameworks (MOFs) possessing many unique features have been utilized in several fields in recent years. However, their application in field emission (FE) vacuum electronic device is hindered by their poor electrical conductivity. Herein, a novel conductive MOF of Cu-catecholate (Cu-CAT) with the nanorod length of 200 nm and conductivity of 0.01 S/cm is grown on the graphite paper (GP). Under an

applied electric field, a large number of electrons can be emitted from the nanoscale emitter tips of MOF surface to the anode. The great field emission performance of Cu-CAT@GP cold cathode film including a low turn-on field of 0.59 V/ μm and ultra-high field enhancement factor of 29622, even comparable to most carbon-based materials that have been widely investigated in FE studies, is achieved in this work. Meanwhile, Cu-CAT@GP film has a good electrical stability with a current attenuation of 9.4% in two hours. The findings reveal the cathode film fabricated by conductive MOF can be a promising candidate of cold electron source for vacuum electronic applications.

Keywords: MOF, Cu-CAT, conductivity, field emission, vacuum electronic device.

1. Introduction

Metal-organic frameworks (MOFs), consisting of metal ions and organic ligands, have attracted increasing attention owing to their porous structure, tunable pore size, numerous metal-containing active redox sites and high surface areas [1-4]. In view of their superior properties, many researches on MOFs are carried out in different fields, such as gas separation/desorption [5], sensing [6], energy storage [7, 8] and adsorption [9, 10]. However, most of the conventional MOFs are severely confined in some

electrical or electrochemical applications because of their weak conductivity ($<10^{-6}$ S/cm) [11]. Their utilizations in electrode material applications have been limited to only serving as precursors/templates of porous carbons and metal oxides, or composites with other conductive materials such as carbon nanotubes (CNTs), graphene, conductive polymers, etc. [12-16] These strategies usually not only sacrifice the inherent large surface area and natural pores of MOFs, but also lead to complex synthesis. Thus, it is significant to fabricate novel MOFs which can be utilized as electrodes themselves and avoid complicated synthetic procedures. In recent years, several conductive MOFs have been investigated [17-19]. For example, the conductive MOF named Cu-catecholate (Cu-CAT) with outstanding conductivity (up to 0.2 S/cm) was first reported by Yaghi with his co-workers in 2012 [19]. Compared to conventional MOFs with poor conductivity, three electron transfer pathways can be envisaged in conductive MOFs, including through-space, through-bond and through-guest conduction [20].

A few conductive MOFs, as yet, have been directly used in oil/water separation, supercapacitors and lithium-ion batteries [21-23]. With their good conductivity and other splendid properties, field emission device (FED), a quantum tunnelling vacuum electronic device, is one of potential applications of the conductive MOFs [24, 25]. Up

to now, FEDs have been investigated in several fields, such as field emission displays [25], microwave devices [26], ionic wind generators [27, 28] and triboelectric nanogenerators [29, 30]. Cold cathode, serving as an electron source, is the core of field emission devices. In the past few decades, many cathode materials such as metal molybdenum, metal oxides, carbon materials (carbon nanotubes, SiC and graphene), the MXene materials and so on have been explored and investigated [31-37]. Nevertheless, there is no research on the application of MOF materials in the field emission.

Herein, our experiment focused on the possibility of conductive MOF (Cu-CAT) application in the field of FE. We chose graphite paper (GP) as the substrate to grow Cu-CAT for the first time because of its high electrical conductivity, thermal conductivity and relatively low price comparing with substrates for Cu-CAT growth previously reported [38, 39]. As a consequence, a thin film of conductive Cu-CAT nanorods was grown on the GP and demonstrated excellent FE performance comparable with popular FE cathodes of carbon-based materials. The work provides a new direction for the selection of FE cathode materials and shows great potential for the development of FE devices.

2. Experimental section

The fabrication procedure of the conductive Cu-CAT nanorod cathode in this work is schematically shown in Fig. 1a. Similar to a typical procedure [40], copper acetate monohydrate (12 mg, 0.06 mmol) and HHTP (2,3,6,7,10,11-Hexahydroxytriphenylene) (9.8 mg, 0.03 mmol) were dispersed in 1 mL solvent mixture of deionized water/DMF (N, N-Dimethylformamide) (v: v = 1:1) under sonication for 15 min in a 10 ml teflon-lined stainless-steel autoclave. Note that in order that the reactants can be uniformly dispersed on the graphite paper serving as a substrate for growth of Cu-CAT nanorods, the solution continued to be sonicated for 10 minutes after the graphite paper was submerged into the reactant solution. The autoclave was then heated in an oven at the temperature of 85 °C for the crystallization to occur. After 24 h of reaction, the reactor was cooled to room temperature and the dark colored product grown on the graphite paper was achieved. The MOF nanorods coated graphite paper was then washed with deionized water for three times and subsequently treated by freeze-drying technique.

For the purpose of forming a complete cathode, it is also necessary to glue the coated graphite paper and fluorine-doped tin oxide (FTO) glass with double-sided conductive adhesive [41]. Next, the Cu-CAT cathode was assembled into a field emission device as one part of it. The inset in Fig. 4a shows the cross-section view of

the FED. The FTO glass as anode was coated with a layer of phosphor to explore its luminescence properties. The distance between the cathode and anode of the FED was controlled at 990 μm .

3. Results and discussion

Fig. 1b shows the crystal structure of Cu-CAT. Each Cu ion coordinates with two adjacent 2,3,6,7,10,11-hexahydroxytriphenylene (HHTP) ligands to form a two-dimensional (2D) hexagonal lattice on the ab plane by virtue of honeycomb-like porous structure formed by π -stacking and π -conjugation. Effective orbital overlap between Cu ions and organic ligands makes Cu-CAT own good charge transfer characteristics [39].

The scanning electron microscopy (SEM) images in Fig. 1c-e illustrate the morphology of graphite paper and Cu-CAT nanorods grown on graphite paper (Cu-CAT@GP) respectively. Fig. 1c shows the graphite paper is composed of rolled graphite flakes, which contain numerous sharp edges in the microstructure. According to the Fig. 1d, it demonstrates that most MOF nanorods are tightly stacked together near the edge of the graphite sheet. Fig. S1a-c show the growth of Cu-CAT on graphite paper at different reaction times under the same hydrothermal conditions. The length of Cu-CAT nanorods can be controlled by reaction time. As shown in Fig. 1e, Cu-CAT can grow to

200 nm in length on graphite paper after hydrothermal reaction for 24 h. Note that the shape of Cu-CAT nanorods has been reported previously, while the Cu-CAT grown on graphite paper has a larger diameter and a shorter length [42]. Moreover, Cu, O and C elements are all detected from energy dispersive X-ray spectroscopy (EDS) elemental mapping images (Fig. S2a-c). The content ratio of O atom to Cu atom is 4.19:1 (Fig. S2d and Table S1), which is close to the Cu-CAT ($C_{36}H_{12}O_{12}Cu_3$) theoretical value ratio of 4:1, revealing that a thin film of Cu-CAT has been coated on graphite paper. The transmission electron microscope (TEM) image of the Fig. 2a demonstrates the stacked rod-like structure of Cu-CAT with a diameter of approximately 45 nm. In the Fig. 2b, a clear lattice strip with a spacing of 0.336 nm between Cu-CAT (002) crystal plane is observed.

Fig. 2c illustrates the X-ray diffraction (XRD) pattern of Cu-CAT nanorods. Note that the diffraction peak intensity of graphite paper in the region of 2θ between 25.5° and 27.5° is too strong to display. All diffraction peaks located at 4.7° , 9.5° , 12.6° , 16.5° , and 27.7° match well with the XRD patterns of Cu-CAT powder and simulated diffraction peaks, illustrating that the Cu-CAT nanorods grown on the graphite paper have similar crystal structure and crystallinity with the reported Cu-CAT [42]. The peak of (002) located at 27.7° corresponds to an interlayer spacing of 0.322 nm according to

the well-known Bragg equation, which is similar to the value of (002) spacing analyzed from TEM image of Cu-CAT.

For the further investigation of specific surface chemical states of Cu-CAT nanorods, X-ray photoelectron spectroscopy (XPS) measurement was also performed. As shown in Fig. 2d, the main element peaks centered at binding energies (BEs) of 285.17, 532.7 and 935.08 eV are attributed to C1s, O1s, and Cu2p, respectively. The element peak centered at BE of 400.62 eV is attributed to N1s, which probably derives from a very small amount of residual DMF. The spectrum of C1s (Fig. S3) can be deconvoluted into four peaks at BEs of 284.4, 284.8, 285.5 and 287.1 eV, corresponding to C=C, C-C, C-O and C=O, respectively [43]. The O1s spectrum (Fig. 2e) can be fitted into three peaks at 531.6, 532.3 and 533.1 eV, respectively assigned to O-Cu, O-C and O=C [44]. Fig. 2f shows the high-resolution Cu 2p spectrum of Cu-CAT nanowires. The peaks located at BE of 934.6 eV (Cu 2p_{3/2}) and 954.6 eV (Cu 2p_{1/2}), and the shake-up satellite (Sat.) peaks in 938.9-947.4 eV are the characteristic peaks of Cu²⁺ [40]. The nitrogen sorption results and the corresponding pore size distribution of Cu-CAT (Fig. S4a, b) shows that the nanorods possess a large Brunauer–Emmett–Teller (BET) specific surface area of 229 m²/g and narrow pore size distribution of 0.9-1.2 nm.

The electronic property of Cu-CAT was featured by work function measurement

using ultraviolet photoelectron spectroscopy (UPS). The work function is an important factor influencing FE performance [45]. Fig. 3a shows the UPS spectra of Cu-CAT nanorods having corrected bias. We find that the work function of synthesized Cu-CAT nanorods deposited on graphite paper is equal to 5.84 eV, determined from the secondary electron cut-off, similar to the reported values of 5.99 eV [46]. Such difference in work function could be attributed to the different synthesis environment that affects the surface state. The determination of the valence band (VB) edge is also an important parameter for band energy alignment diagram, as presented in Fig. 3b, VB edge value estimated of Cu-CAT is 1.79 eV. The energy diagram in Fig. 3c schematizes the work function and ionization energy reduction of Cu-CAT.

The electrical conductivity can also impact the FE performance. To some extent, the conductivity represents the ability of the cathode material to transfer electrons to the field emitters and generate electron beams. A cold cathode with higher electrical conductivity tends to have better FE performance. In our previous work, the field emission performance of SiC nanowire cathode was enhanced by adding conductive polymers to increase the conductivity of SiC [47]. The electrical conductivity of Cu-CAT nanorods in this work is measured to be 0.01 S/cm, similar to the conductivity of Cu-CAT reported before [48]. As a part of cathode film, graphite paper (measured to be

2564 S/cm) with high conductivity can quickly transport carriers to emission tips of Cu-CAT nanorods and emit electron beams under external voltage, so as to obtain excellent field emission performance.

To explore the field emission performance, the current density versus applied electric field (J - E) plot for field emission characteristics of the Cu-CAT nanorods cathode is shown in Fig. 4a. Turn-on field (E_{on} , defined at a current density of 10 $\mu\text{A}/\text{cm}^2$) and threshold field (E_{th} , defined at a current density of 100 $\mu\text{A}/\text{cm}^2$) are 0.59 and 0.81 V/ μm , respectively. These values are best among the state-of-the-art reported devices [36,41,49]. As is known, field emission cathode materials often have protrusions in the microscopic morphology, which make them play a role in greatly enhancing the local electric field in field emission. The relationship between the local electric field (E_{local}) and the applied electric field (E) can be described as $E_{\text{local}} = \beta E$, where β , the field enhancement factor, is also one of important factors for judging field emission performance. It can be calculated by Fowler–Nordheim (F–N) theory [50] which is described by

$$J = A\Phi^{-1}\beta^2 e^2 \exp\left(-\frac{B\Phi^{\frac{3}{2}}}{\beta E}\right), \quad (1)$$

where both A and B are constants, corresponding to $1.54 \times 10^{-6} \text{ A}\cdot\text{eV}\cdot\text{V}^{-2}$ and $6.83 \times 10^3 \text{ V}\cdot\text{eV}^{3/2}\cdot\mu\text{m}^{-1}$, respectively, and ϕ is the work function of the cathode (5.84 eV in

this study). The F–N plot of Cu-CAT nanorods (Fig. S5) displays the value of β can be calculated as 29622 according to the slope of the plot.

As shown in Fig. 4b and Table S2, compared with several field emission performances of newly reported cathode materials, Cu-CAT surpasses most of its counterparts in the list. It can be even comparable to some carbon-based materials such as CNTs and SiC, which are always considered as popular candidates for field emission cathodes.

In addition, we also studied the device stability of Cu-CAT nanorod cathode. The field emission stability has been shown in Fig. 5a and the original current density was set to 100 $\mu\text{A}/\text{cm}^2$. According to the plot where the normalized current density changes with time, the current density has no obvious degradation within 120 minutes. The current density decreased from 100 to 90.6 $\mu\text{A}/\text{cm}^2$, with an attenuation of 9.4%. Moreover, the illustrations of insets in Fig. 5a show the luminous uniformity of sample and the current fluctuation range concentrated within $\pm 20\%$ which demonstrates the MOF-FED has a pretty good stability in vacuum compared with recent reports [34,51]. Meanwhile, no obvious change of Cu–CAT@GP's XRD pattern can be found before and after field emission test, indicating the excellent stability of the MOF cathode in FED under vacuum. This can be partly attributed to graphite paper. As the substrate for

growing Cu-CAT nanorods and one part of the cathode material film, the graphite paper with good thermal conductivity can make the field emission cathode weaken the influence of thermal effect caused by high current density reducing the damage to the morphology and microstructure, and thus improve the stability.

A comparison of the feasibility of previously reported different substrates used to grow Cu-CAT and the graphite paper used in this work is shown in Table S3, indicating that graphite paper has great advantages in terms of electrical conductivity, thermal conductivity, and price.

4. Conclusions

In summary, we fabricated stacked Cu-CAT nanorods grown on graphite paper from bottom to top through a hydrothermal synthesis method. Compared with other common substrates for growing Cu-CAT nanorods, the graphite paper used in this study is not only relatively inexpensive but also has good electrical and thermal conductivity. The Cu-CAT film grown on graphite paper (Cu-CAT@GP film) has a large specific surface area (229 m²/g), small pore size (0.9-1.2 nm) and high electrical conductivity (0.01 S/cm). Moreover, outstanding field emission performance of the conductive MOFs is proved. Because of their rod-like one-dimensional (1D) structure and good

conductivity, Cu-CAT nanorods possess splendid FE properties. Their turn-on and threshold applied fields can be 0.59 and 0.81 V/ μm , respectively. Simultaneously, it also owns high field enhancement factor of 29622 and great current stability. These findings reveal that conductive metal-organic framework can be also a promising candidate for vacuum electronic devices.

Conflicts of interest

There are no conflicts to declare.

Acknowledgements

This work was financially supported by National Natural Science Foundation of China (Grant No. 61771198) and Natural Science Foundation of Shanghai (Grant No. 17ZR1447000). We acknowledge Prof. S. Liu and Prof. M. Hu at East China Normal University, Shanghai, China for their help in material preparation and characterization.

References

1. G. Skorupskii, B. A. Trump, T. W. Kasel, C. M. Brown, C. H. Hendon and M. Dincă, Efficient and tunable one-dimensional charge transport in layered lanthanide metal–organic frameworks, *Nat. Chem.*, 12 (2020) 131-136.

<https://doi.org/10.1038/s41557-019-0372-0>

2. B. L. Bonnett, E. D. Smith, M. De La Garza, M. Cai, J. V. Haag, J. M. Serrano, H. D. Cornell, B. Gibbons, S. M. Martin and A. J. Morris, PCN-222 Metal–Organic Framework Nanoparticles with Tunable Pore Size for Nanocomposite Reverse Osmosis Membranes, *ACS Appl. Mater. Interfaces*, 12 (2020) 15765-15773.

<https://doi.org/10.1021/acsami.0c04349>

3. G. Pena-Velasco, L. Hinojosa-Reyes, G.A. Moran-Quintanilla, A. Hernandez-Ramirez, M. Villanueva-Rodriguez, J.L. Guzman-Mar, Synthesis of heterostructured catalyst coupling MOF derived Fe₂O₃ with TiO₂ for enhanced photocatalytic activity in anti-inflammatory drugs mixture degradation, *Ceram. Int.*, 47 (2021) 24632-24640.

<https://10.1016/j.ceramint.2021.05.185>

4. X. J. Zhang, W. Ou-Yang, G. Zhu, T. Lu and L. K. Pan, Shuttle-like carbon-coated FeP derived from metal-organic frameworks for lithium-ion batteries with superior rate capability and long-life cycling performance, *Carbon*, 143 (2019) 116-124.

<https://doi.org/10.1016/j.carbon.2018.11.005>

5. J. R. Li, R. J. Kuppler and H. C. Zhou, Selective gas adsorption and separation in metal-organic frameworks, *Chem. Soc. Rev.*, 38 (2009) 1477-1504.

<https://doi.org/10.1039/B802426J>

6. F. Zhang, J.L. Zhang, J. Song, Y. You, X.L. Jin, J.J. Ma, Anchoring Ni-MOF nanosheet on carbon cloth by zeolite imidazole framework derived ribbonlike Co₃O₄ as integrated composite cathodes for advanced hybrid supercapacitors, *Ceram. Int.*, 47 (2021) 14001-14008.

<https://10.1016/j.ceramint.2021.01.269>

-
7. N. A. A. Qasem, R. Ben-Mansour and M. A. Habib, An efficient CO₂ adsorptive storage using MOF-5 and MOF-177, *Appl. Energy*, 210 (2018) 317-326.
<https://doi.org/10.1016/j.apenergy.2017.11.011>
 8. J. W. Ren, N. M. Musyoka, P. Annamalai, H. W. Langmi, B. C. North and M. Mathe, Electrospun MOF nanofibers as hydrogen storage media, *Int. J. Hydrogen Energy*, 40 (2015) 9382-9387.
<https://doi.org/10.1016/j.ijhydene.2015.05.088>
 9. N. Al-Janabi, P. Hill, L. Torrente-Murciano, A. Garforth, P. Gorgojo, F. Siperstein and X. Fan, Mapping the Cu-BTC metal–organic framework (HKUST-1) stability envelope in the presence of water vapour for CO₂ adsorption from flue gases, *Chem. Eng. J.*, 281 (2015) 669-677.
<https://doi.org/10.1016/j.cej.2015.07.020>
 10. Y. Zhang, S. Yuan, X. Feng, H. Li, J. Zhou and B. Wang, Preparation of Nanofibrous Metal-Organic Framework Filters for Efficient Air Pollution Control, *J. Am. Chem. Soc.*, 138 (2016) 5785-5788.
<https://doi.org/10.1021/jacs.6b02553>
 11. M.H. Hassan, M.H. Alkordi, A. Hassanien, Probing the conductivity of metal-organic framework-graphene nanocomposite, *Mater. Lett.*, 246 (2019) 13-16.
<https://doi.org/10.1016/j.matlet.2019.02.124>
 12. S. Rani, B. Sharma, R. Malhotra, S. Kumar, R. S. Varma and N. Dilbaghi, Sn-MOF@CNT nanocomposite: An efficient electrochemical sensor for detection of hydrogen peroxide, *Environ. Res.*, 191 (2020) 110005.
<https://doi.org/10.1016/j.envres.2020.110005>
 13. M. Jahan, Q. L. Bao and K. P. Loh, Electrocatalytically Active Graphene-

Porphyrin MOF Composite for Oxygen Reduction Reaction, *Journal of the American Chemical Society*, *J. Am. Chem. Soc.*, 134 (2012) 6707-6713.

<https://doi.org/10.1021/ja211433h>

14. Y. Jiao, G. Chen, D. H. Chen, J. Pei and Y. Y. Hu, Bimetal-organic framework assisted polymerization of pyrrole involving air oxidant to prepare composite electrodes for portable energy storage, *J. Mater. Chem. A*, 5 (2017) 23744-23752.
<https://doi.org/10.1039/c7ta07464f>
15. Y. An, Y. Tian, Y. Li, C. Wei, Y. Tao, Y. Liu, B. Xi, S. Xiong, J. Feng and Y. Qian, Heteroatom-doped 3D porous carbon architectures for highly stable aqueous zinc metal batteries and non-aqueous lithium metal batteries, *Chem. Eng. J.*, 400 (2020) 125843.
<https://doi.org/10.1016/j.cej.2020.125843>
16. J. Feng, L. Liu and Q. Meng, Enhanced electrochemical and capacitive deionization performance of metal organic framework/holey graphene composite electrodes, *J. Colloid Interface Sci.*, 582 (2021) 447-458.
<https://doi.org/10.1016/j.jcis.2020.08.091>
17. Z. J. Chen, Y. T. Cui, Y. G. Jin, L. Y. Liu, J. Yan, Y. Sun, Y. Zou, Y. M. Sun, W. Xu and D. B. Zhu, Nanorods of a novel highly conductive 2D metal-organic framework based on perthiolated coronene for thermoelectric conversion, *J. Mater. Chem. C*, 8 (2020) 8199-8205.
<https://doi.org/10.1039/D0TC01778G>
18. K. Yuan, T. Song, C. Yang, J. Guo, Q. Sun, Y. Zou, F. Jiao, L. Li, X. Zhang, H. Dong, L. Li, W. Hu, Polymer-Assisted Space-Confined Strategy for the Foot-Scale Synthesis of Flexible Metal-Organic Framework-Based Composite Films, *J. Am.*

-
- Chem. Soc.*, 143 (2021) 17526-17534.
<https://doi.org/10.1021/jacs.1c07033>
19. M. Hmadeh, Z. Lu, Z. Liu, F. Gándara, H. Furukawa, S. Wan, V. Augustyn, R. Chang, L. Liao, F. Zhou, E. Perre, V. Ozolins, K. Suenaga, X. Duan, B. Dunn, Y. Yamamoto, O. Terasaki and O. M. Yaghi, New Porous Crystals of Extended Metal-Catecholates, *Chem. Mater.*, 24 (2012) 3511-3513.
<https://doi.org/10.1021/cm301194a>
20. J. Nyakuchena, S. Ostresh, D. Streater, B. Pattengale, J. Neu, C. Fiankor, W. Hu, E. D. Kinigstein, J. Zhang, X. Zhang, C. A. Schmittenmaer and J. Huang, Direct Evidence of Photoinduced Charge Transport Mechanism in 2D Conductive Metal Organic Frameworks, *J. Am. Chem. Soc.*, 142 (2020) 21050-21058.
<https://doi.org/10.1021/jacs.0c09000>
21. Y. Yin, L. Zhu, T. Guo, X. Qiao, S. Gan, X. Chang, X. Li, F. Xia and Q. Xue, Microphone-like Cu-CAT-1 hierarchical structures with ultra-low oil adhesion for highly efficient oil/water separation, *Separation and Purification Technology, Sep. Purif. Technol.*, 241 (2020) 116688.
<https://doi.org/10.1016/j.seppur.2020.116688>
22. W. Zhou, S. Lv, X. Liu, Y. Li and J. Liu, A directly grown pristine Cu-CAT metal-organic framework as an anode material for high-energy sodium-ion capacitors, *Chem. Commun.*, 55 (2019) 11207-11210.
<https://doi.org/10.1039/c9cc06048k>
23. Y. F. Wang, S. Y. Yang, Y. Yue and S. W. Bian, Conductive copper-based metal-organic framework nanowire arrays grown on graphene fibers for flexible all-solid-state supercapacitors, *J. Alloys Compd.*, 835 (2020) 155238.

<https://doi.org/10.1016/j.jallcom.2020.155238>

24. J. H. Booske, R. J. Dobbs, C. D. Joye, C. L. Kory, G. R. Neil, G. S. Park, J. Park and R. J. Temkin, Vacuum Electronic High Power Terahertz Sources, *IEEE Trans Terahertz Sci Technol*, 1 (2010) 54-75.

<https://doi.org/10.1109/TTHZ.2011.2151610>

25. J. Z. Xu, P. Xu, P. S. Guo, W. Ou-Yang, Y. W. Chen, T. Feng, X. Q. Piao, M. Wang and Z. Sun, All carbon nanotube based flexible field emission devices prepared through a film transfer method, *RSC Adv.*, 5 (2015) 21755-21761.

<https://doi.org/10.1039/c4ra16095a>

26. K. B. K. Teo, E. Minoux, L. Hudanski, F. Peauger, J.-P. Schnell, L. Gangloff, P. Legagneux, D. Dieumegard, G. A. J. Amaratunga and W. I. Milne, Microwave devices: carbon nanotubes as cold cathodes, *Nature*, 437 (2005) 968.

<https://doi.org/10.1038/437968a>

27. Y. S. Wu, J. Li, J. C. Ye, X. H. Chen, H. L. Li, S. M. Huang, R. Zhao and W. Ou-Yang, Greener corona discharge for enhanced wind generation with a simple dip-coated carbon nanotube decoration, *J. Phys. D: Appl. Phys.*, 50 (2017) 395304.

<https://doi.org/10.1088/1361-6463/aa81a9>

28. J. Ye, J. Li, X. Chen, S. Huang, W. Ou-Yang, Enhancement of corona discharge induced wind generation with carbon nanotube and titanium dioxide decoration, *Chinese Phys. B*, 28 (2019) 095202.

<http://dx.doi.org/10.1088/1674-1056/ab33ed>

29. X. Y. Chen, T. Jiang, Z. Sun and W. Ou-Yang, Field emission device driven by self-powered contact-electrification: Simulation and experimental analysis, *Appl. Phys. Lett.*, 107 (2015) 114103.

<https://doi.org/10.1063/1.4931463>

30. B. Yang, J. Chen, X. Wu, B. Liu, L. Liu, Y. Tang and X. Yan, Enhanced field emission performance of MXene-TiO₂ composite films *Nanoscale*, 13 (2021) 7622-7629.

<https://doi.org/10.1039/d0nr08900a>

31. G. Deokar, N.S. Rajput, J. Li, F.L. Deepak, W. Ou-Yang, N. Reckinger, C. Bittencourt, J.F. Colomer, M. Jouiad, Toward the use of CVD-grown MoS₂ nanosheets as field-emission source, *Beilstein J. Nanotechnol.*, 9 (2018) 1686-1694.

<https://doi.org/10.1002/sml.201300002>

32. Z.W.I. Kwek, Y.J.V. Tan, Z. Zhang, C.-H. Sow, S.X. Lim, Scintillating zinc oxide ensconced in a carbon nanotube forest engineered by laser micro-welding, *Appl. Surf. Sci.*, 562 (2021) 150231.

<https://doi.org/10.3762/bjnano.9.160>

33. U. N. Maiti, S. Nandy, S. Karan, B. Mallik and K. K. Chattopadhyay, Enhanced optical and field emission properties of CTAB-assisted hydrothermal grown ZnO nanorods, *Appl. Surf. Sci.*, 254 (2008) 7266-7271.

<https://doi.org/10.1016/j.apsusc.2008.05.311>

34. H. Wu, S. Shen, X. Xu, C. Qiao, X. Chen, J. Li, W. Li, W. Ou-Yang, Facile Fabrication and High Field Emission Performance of 2-D Ti₃C₂T_x MXene Nanosheets for Vacuum Electronic Devices, *IEEE Trans. Electron Devices*, 67 (2020) 5138-5143.

<https://doi.org/10.1109/ted.2020.3021625>

35. C. Qiao, H. Wu, X. Xu, Z. Guan, W. Ou-Yang*, Electrical Conductivity

Enhancement and Electronic Applications of 2D Ti₃C₂T_x MXene Materials, *Adv. Mater. Interfaces*, 2021, 8 (24), 2100903

36. J. Z. Xu, P. Xu, W. Ou-Yang, X. H. Chen, P. S. Guo, J. Li, X. Q. Piao, M. Wang and Z. Sun, Outstanding field emission properties of wet-processed titanium dioxide coated carbon nanotube based field emission devices, *Appl. Phys. Lett.*, 106 (2015) 073501.
<https://doi.org/10.1063/1.4909552>
37. D. Wu, Y. Chen, X. Hong, L. Wang, W. Ou-Yang, S. Tao, Q. Zhao, B. Qian, P.K. Chu, Field emission from geometrically modulated tungsten-nickel sulfide / graphitic carbon nanobelts on Si microchannel plates, *Ceram. Int.*, 47 (2021) 4034-4042.
<https://doi.org/10.1016/j.ceramint.2020.09.270>
38. W.-H. Li, K. Ding, H.-R. Tian, M.-S. Yao, B. Nath, W.-H. Deng, Y. Wang and G. Xu, Conductive Metal-Organic Framework Nanowire Array Electrodes for High-Performance Solid-State Supercapacitors, *Adv. Funct. Mater.*, 27 (2017) 1702067.
<https://doi.org/10.1002/adfm.201702067>
39. R. Hou, M. Miao, Q. Wang, T. Yue, H. Liu, H. S. Park, K. Qi and B. Y. Xia, Integrated Conductive Hybrid Architecture of Metal-Organic Framework Nanowire Array on Polypyrrole Membrane for All-Solid-State Flexible Supercapacitors, *Adv. Energy Mater.*, 10 (2019) 1901892.
<https://doi.org/10.1002/aenm.201901892>
40. L. Guo, J. Sun, W. Zhang, L. Hou, L. Liang, Y. Liu and C. Yuan, Bottom-Up Fabrication of 1D Cu-based Conductive Metal-Organic Framework Nanowires as a High-Rate Anode towards Efficient Lithium Storage, *ChemSusChem*, 12 (2019)

5051-5058.

<https://doi.org/10.1002/cssc.201902194>

41. C. Yi, H. Wu, J. Li, Y. Song, Y. Song, X. Chen, W. Ou-Yang, Crack-Assisted Field Emission Enhancement of Carbon Nanotube Films for Vacuum Electronics, *ACS Appl. Nano Mater.*, 2 (2019) 7803-7809.
<https://doi.org/10.1021/acsanm.9b01830>
42. X. Ma, Z. Li, Z. Deng, D. Chen, X. Wang, X. Wan, Z. Fang, X. Peng, Efficiently cogenerating drinkable water and electricity from seawater via flexible MOF nanorod arrays, *J. Mater. Chem. A*, 9 (2021) 9048-9055.
<https://doi.org/10.1039/d0ta11870b>
43. B. M. Abu-Zied, M. A. Hussein, A. Khan and A. M. Asiri, Cu-Cu₂O@graphene nanoplatelets nanocomposites: Facile synthesis, characterization, and electrical conductivity properties, *Mater. Chem. Phys.*, 213 (2018) 168-176.
<https://doi.org/10.1016/j.matchemphys.2018.04.036>
44. Ö. Karahan, E. Biçer, A. Taşdemir, A. Yürüm and S. A. Gürsel, Development of Efficient Copper-Based MOF-Derived Catalysts for the Reduction of Aromatic Nitro Compounds, *Eur. J. Inorg. Chem.*, 2018 (2018) 1073-1079.
<https://doi.org/10.1002/ejic.201701320>
45. Y. Song, J. Li, W. Ou-Yang, Thickness Effect on Field-Emission Properties of Carbon Nanotube Composite Cathode, *IEEE Trans. Electron Devices*, 66 (2019) 716-721.
<https://doi.org/10.1109/ted.2018.2878738>
46. M. S. Yao, X. J. Lv, Z. H. Fu, W. H. Li, W. H. Deng, G. D. Wu and G. Xu, Layer-by-Layer Assembled Conductive Metal-Organic Framework Nanofilms for

-
- Room-Temperature Chemiresistive Sensing, *Angew. Chem. Int. Ed.*, 56 (2017) 16510-16514.
<https://doi.org/10.1002/anie.201709558>
47. H. Wu, S. Shen, J. Li, X. Chen, Z. Zhang and W. Ou-Yang, Boosted field emission properties and thickness effect of conductive polymers coated silicon carbide matrices for vacuum electronic devices, *Vacuum*, 180 (2020) 109594.
<https://doi.org/10.1016/j.vacuum.2020.109594>
48. G. X. Zhang, L. Jin, R. X. Zhang, Y. Bai, R. M. Zhu and H. Pang, Recent advances in the development of electronically and ionically conductive metal-organic frameworks, *Coord. Chem. Rev.*, 439 (2021) 213915.
<https://doi.org/10.1016/j.ccr.2021.213915>
49. L. Zhao, S. Chen, L. Wang, F. Gao, X. Yao, W. Yang, Large-scale fabrication of free-standing and transparent SiC nanohole array with tailored structures, *Ceram. Int.*, 44 (2018) 7280-7285
<https://doi.org/10.1016/j.ceramint.2017.12.196>
50. Y. Wu, J. Li, J. Ye, Y. Song, X. Chen, S. Huang, Z. Sun, W. Ou-Yang, Outstanding field emission properties of titanium dioxide /carbon nanotube composite cathodes on 3D nickel foam, *J. Alloys Compd.*, 726 (2017) 675-679.
<https://doi.org/10.1016/j.jallcom.2017.08.026>
51. Yujie Song, Jun Li, Qiang Wu, Chunrong Yi, Han Wu, Zhangyi Chen, Wei Ou-Yang, Study of film thickness effect on carbon nanotube based field emission devices, *J. Alloys Compd.*, 816 (2020) 152648.
<https://doi.org/10.1016/j.jallcom.2019.152648>

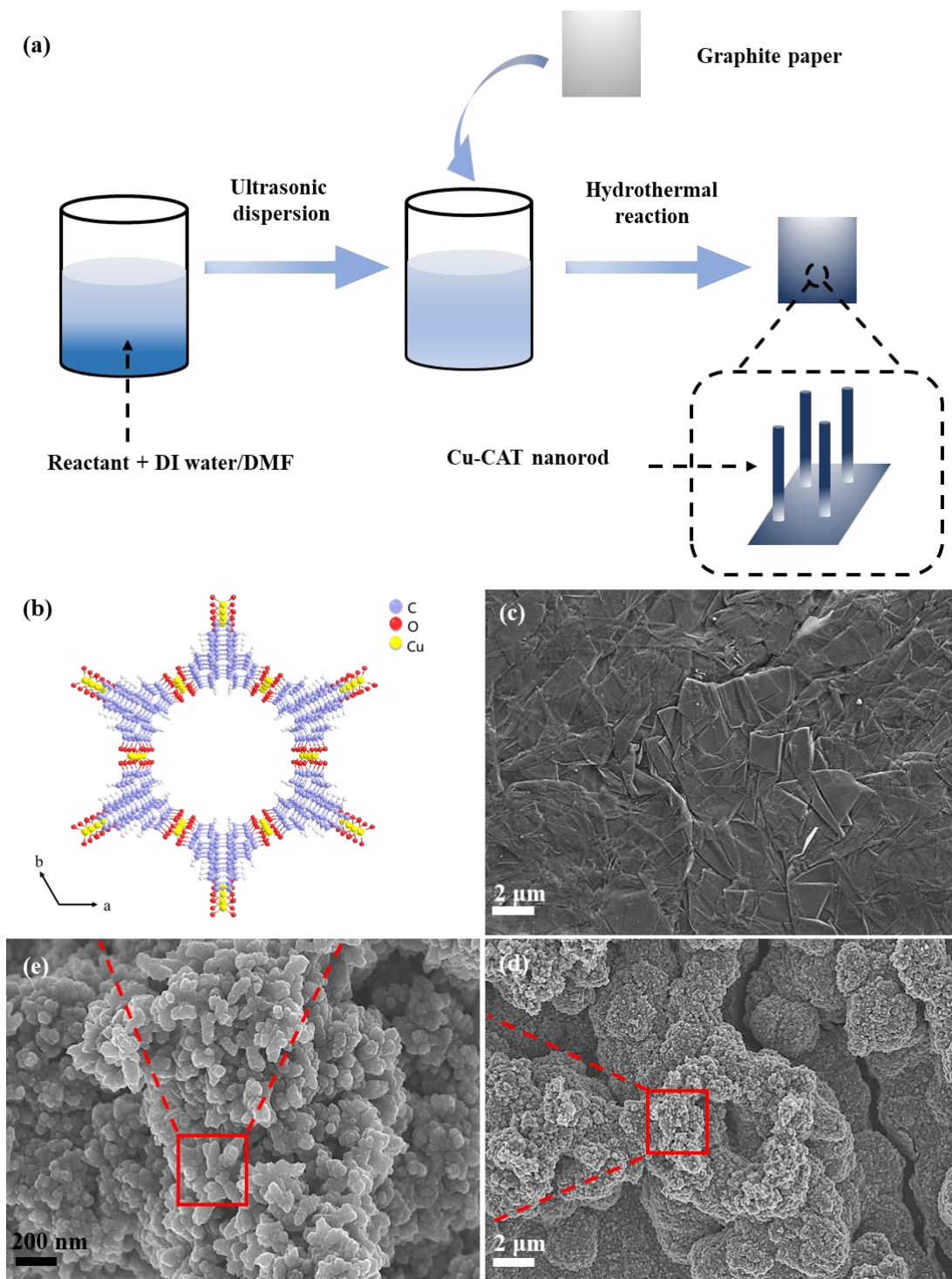


Fig. 1 (a) Preparation illustration of Cu-CAT@GP. (b) The simulated crystal structure of Cu-CAT along the c-axis. (c) SEM of the graphite paper. (d and e) SEM of rough Cu-CAT nanorods grown on graphite paper.

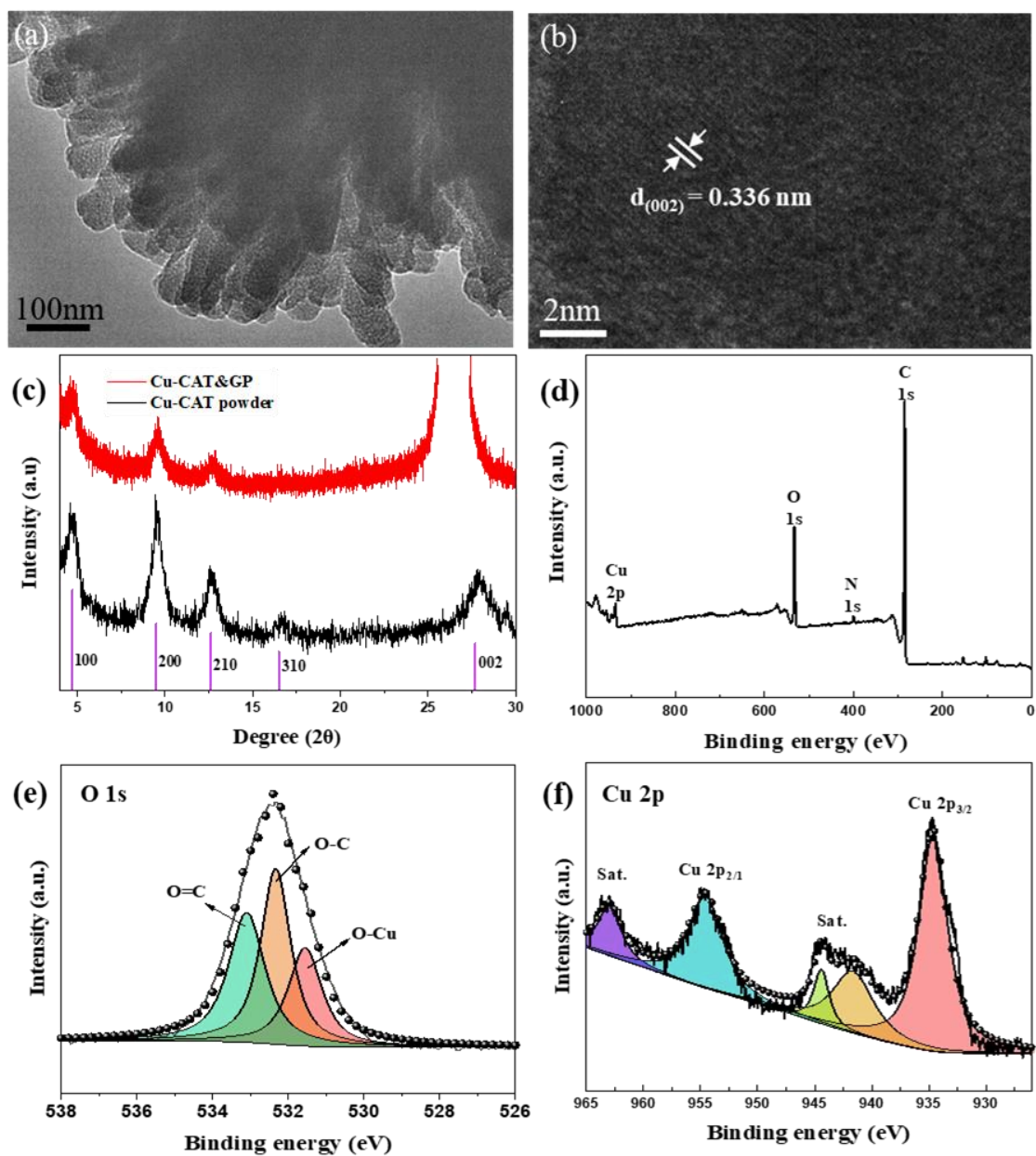


Fig. 2 (a and b) TEM images of Cu-CAT rough nanorods. (c) XRD patterns for Cu-CAT. (d) XPS survey spectrum of Cu-CAT. (e and f) High-resolution XPS spectra of O 1s and Cu 2p, respectively.

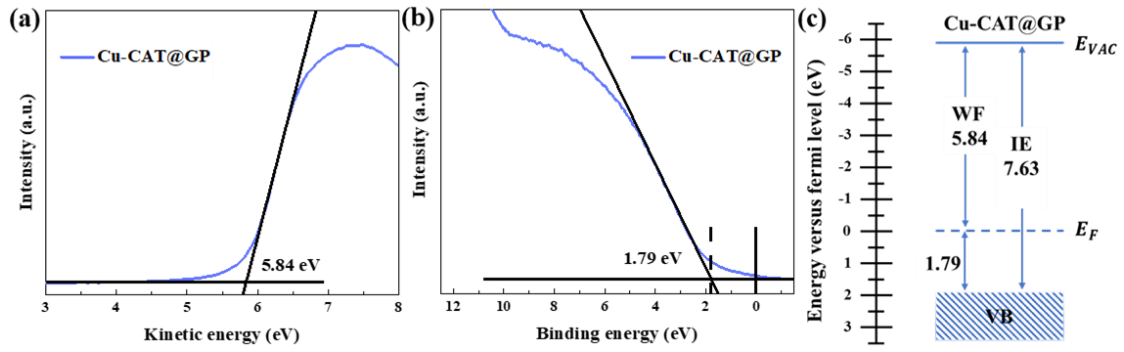


Fig. 3 (a) UPS spectrum around the secondary electron cut-off of Cu-CAT. (b) UPS spectrum in the valence band (VB) region of Cu-CAT. (c) Energy scheme for Cu-CAT with respect to the E_F . IE, ionization energy. E_F , Fermi level. E_{VAC} , vacuum level. WF, work function.

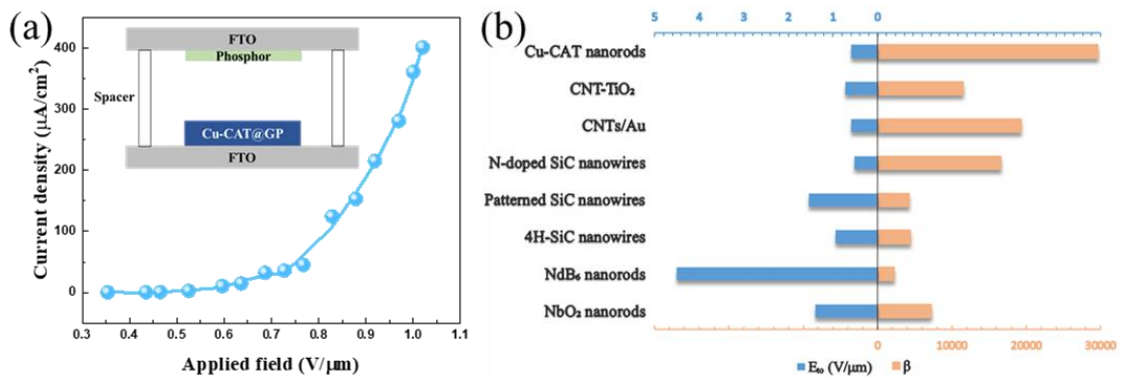


Fig. 4 (a) The typical $J-E$ curve of Cu-CAT@GP and cross-section view of the FED (inset in a). (b) Field emission performance comparison of Cu-CAT nanorods and recent reported 1D nanostructured emitters.

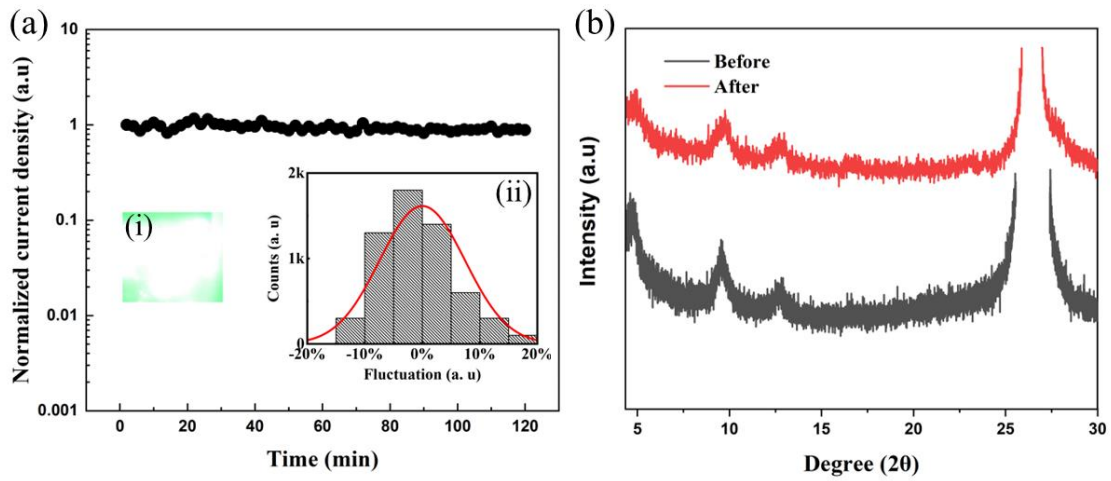


Fig. 5 (a) Field emission stability of Cu-CAT@GP cathode; inset (i) is luminescence picture of FED with Cu-CAT@GP cathode; inset (ii) is frequency histogram and normalized curve of current density fluctuation. (b) XRD patterns for the Cu-CAT@GP cathode before and after field emission test.

Highlights

- A conductive MOF film composed of stacked Cu-CAT nanorods with conductivity of 0.01 S/cm is fabricated on graphite paper.
- Field emission performance of MOF materials is first demonstrated for the conductive Cu-CAT film.
- The FED presents a pretty low turn-on field of 0.59 V/ μm , comparable with the state-of-the-art CNT-based cathode materials.

Graphical abstract

